Journal for ImmunoTherapy of Cancer

Macrophage sensitivity to bexmarilimab-induced reprogramming is shaped by the tumor microenvironment

Jenna H Rannikko ,[1] Rita Turpin,[1] Pia Boström,[2] Reetta Virtakoivu,[1] Chantal Harth,[1] Akira Takeda,[1] Anselm Tamminen,[3] Ilkka Koskivuo,[3] Maija Hollmén [1]

To cite: Rannikko JH, Turpin R, Boström P, *et al*. Macrophage sensitivity to bexmarilimab-induced reprogramming is shaped by the tumor microenvironment. *Journal for ImmunoTherapy of Cancer* 2025;**13**:e011292. doi:10.1136/jitc-2024-011292

► Additional supplemental material is published online only. To view, please visit the journal online (https://doi.org/10.1136/jitc-2024-011292).

Accepted 26 April 2025

[1]MediCity Research Laboratory and InFLAMES Flagship, University of Turku, Turku, Finland
[2]Department of Pathology, TYKS Turku University Hospital, Turku, Finland
[3]Department of Plastic and General Surgery, TYKS Turku University Hospital, Turku, Finland

Correspondence to
Dr Maija Hollmén; maijal@utu.fi

ABSTRACT

Background Tumor-associated macrophages (TAMs) adapt to the tumor microenvironment (TME), either aiding cancer eradication or promoting tumor growth and immune evasion. To manipulate TAMs therapeutically, a deep understanding of their interaction with the TME is essential. This study explores the responsiveness of TMEs to bexmarilimab, a macrophage reprogramming therapy showing clinical benefit in various solid tumors.

Methods We exploited a breast cancer patient-derived explant culture (PDEC) model to characterize bexmarilimab responses in both tumor and adjacent cancer-free tissues by RNA sequencing and multiplex cytokine profiling. Using single-cell RNA sequencing, spatial transcriptomics, and conditioned media treatment, we further investigated the effects of Clever-1+ macrophages and TME features on bexmarilimab sensitivity.

Results The PDEC model captured key aspects of bexmarilimab's mode of action and validated a gene signature for determining treatment sensitivity. We identified three distinct responses to bexmarilimab in tumors and adjacent cancer-free tissues, shaped by the local microenvironment and macrophage phenotype, origin, and localization. The inflammatory state of the TME emerged as the primary determinant of response. Immune activation occurred in immunologically cold TMEs lacking late-stage activated TAMs, whereas interferon-regulated TMEs exhibited suppressed inflammation. In cancer-free breast tissue, bexmarilimab activated B cell responses independent of treatment sensitivity in the adjacent tumor.

Conclusions These findings reveal the complexity of TAM targeting in cancer and emphasize the need for patient selection to maximize bexmarilimab's efficacy.

WHAT IS ALREADY KNOWN ON THIS TOPIC

⇒ Tumor-associated macrophages (TAMs) play a dual role within the tumor microenvironment (TME), either contributing to antitumor immunity or promoting tumor progression and immune evasion. Therapies targeting TAMs are being explored, but their effectiveness depends heavily on the local immune context and macrophage characteristics. Bexmarilimab, a macrophage reprogramming therapy, has shown clinical promise in treating solid tumors, yet the mechanisms determining its efficacy remain poorly understood.

WHAT THIS STUDY ADDS

⇒ This study provides a detailed analysis of how TMEs respond to bexmarilimab, identifying three distinct response profiles shaped by the inflammatory state, macrophage subtype, and spatial distribution within the tissue. It validates a gene signature determining treatment sensitivity and reveals that immunologically cold TMEs are more responsive to therapy. It also uncovers a unique activation of B cell responses in adjacent cancer-free tissues, independent of tumor sensitivity.

HOW THIS STUDY MIGHT AFFECT RESEARCH, PRACTICE OR POLICY

⇒ These findings highlight the importance of immune profiling and patient selection when considering TAM-targeting therapies such as bexmarilimab. They suggest that response to treatment is not uniform but context-dependent, advocating for the integration of biomarkers and spatial immune features into clinical decision-making. This work may guide future therapeutic strategies and inform the design of more effective, personalized immunotherapies.

BACKGROUND

Given the pivotal role of macrophages in regulating tumor growth, novel macrophage-reprogramming immunotherapies are being developed at an accelerated rate.[1 2] Therapeutics targeting tumor-associated macrophages (TAMs) have thus far faced difficulties because of poor monotherapy efficacy caused by narrow therapeutic windows and incomplete understanding of TAMs.[3] Considering the heterogeneity of TAMs, which display varying phenotypes across different tissue niches, patient-to-patient variation, and distinct origins (monocyte-derived vs embryonic populations), it is crucial to unravel how these factors and the tissue environment influence treatment responses and potential side effects.

Macrophage heterogeneity in cancer is shaped by several factors, including tissue-specific niches, spatial localization within tumors, and macrophage ontogeny. Single-cell omics studies have revealed that TAMs exhibit diverse phenotypes and functions depending on their origin and the tissue in which they reside.[4] Despite such heterogeneity, a pan-cancer atlas of myeloid cells identified common TAM subpopulations across different cancer types, each subpopulation displaying unique gene expression profiles and functional properties depending on the surrounding tumor microenvironment (TME).[5] In breast cancer, TAM heterogeneity is driven by specific tissue territories, leading to different macrophage phenotypes with variable roles in tumor progression or immune modulation.[6] Moreover, spatial analysis of TAM populations in colon cancer revealed that macrophages segregated into different tumor regions can predict distinct clinical outcomes.[7]

Bexmarilimab is a humanized IgG4 antibody targeting the scavenger receptor Clever-1 (also known as Stabilin-1) expressed on immunosuppressive macrophage populations and a subset of endothelial cells.[8] It is currently under clinical development as a macrophage-reprogramming immunotherapy to treat patients with advanced solid tumors (MATINS; NCT03733990) and hematological malignancies (BEXMAB; NCT05428969). Bexmarilimab is very well tolerated (n>200 patients) and shows efficacy (disease stabilization) as monotherapy in selected advanced and metastatic solid tumors, such as breast cancer,[9] and robust objective responses with standard of care in hypomethylating agent-failed myelodysplastic syndrome.[10] By binding Clever-1, bexmarilimab inhibits the scavenging of modified low-density lipoproteins, which reduces the activation of nuclear lipid receptors, and potentiates TNFα release in macrophages after lipopolysaccharide stimulation.[11] Bexmarilimab is rapidly internalized with Clever-1 in endosomes, thereby impairing the multiprotein vacuolar ATPase-mediated acidification of phagolysosomes. This activity enhances the ability of macrophages to cross-present antigens to activate cytotoxic CD8+ T cells.[12] Recent findings from the MATINS trial showed that low baseline immune activation is associated with bexmarilimab benefit, resulting in the activation of intratumoral macrophages, increase in circulating interferon gamma (IFNγ), and prolonged survival.[9]

We previously investigated ovarian cancer ascites cells and observed that chronic IFN exposure inhibited TAM activation by bexmarilimab.[13] However, a comprehensive knowledge of the TME in this context is currently lacking, which is essential for identifying the TMEs where bexmarilimab can effectively reprogram TAMs. This would significantly improve the success of future clinical trials and support patient enrichment strategies considering the immune landscape[14] rather than the tissue of origin of the tumor, thereby opening new possibilities for pan-cancer trials.

To address this gap, we used a patient-derived explant culture (PDEC) model to investigate bexmarilimab responses in breast tumors and their adjacent healthy tissues. Similar models have been previously employed to evaluate anti-PD-1 responses,[15 16] demonstrating their utility in studying immune therapeutic effects. Our analyses revealed that bexmarilimab elicits immune activation in immunologically quiet TMEs but suppresses inflammation in TMEs characterized by IFN signaling and late-stage activated TAMs. In adjacent healthy tissues, bexmarilimab primarily activates B cell responses via tissue-resident macrophages, independently of its sensitivity in the corresponding tumor. This highlights the role of macrophage ontogeny and the inflammatory state of the TME in shaping bexmarilimab response.

METHODS

Human subjects

Samples of tumor and adjacent cancer-free tissue were obtained from patients with breast cancer who underwent mastectomy at Turku University Hospital in Finland. This study included patients with a tumor diameter >2 cm who did not receive neoadjuvant therapy. Matching tumor and adjacent tissue areas were examined by a pathologist to ensure the presence of invasive carcinoma in the tumor specimen and the absence of cancer in the adjacent breast tissue specimen. Tumor or adjacent tissue specimens were collected into RPMI and used freshly, unless otherwise indicated.

The MATINS trial and pretreatment serum IFNγ measurements have been previously described.[9] The patients with estrogen receptor-positive (ER+) breast cancer analyzed here are listed in online supplemental table S1.

Data mining to identify bexmarilimab response genes

To identify genes associated with beneficial bexmarilimab treatment responses, we collected differentially expressed genes (DEGs) from two bexmarilimab treatment datasets, named “MATINS trial” and “Ovarian ascites”. In the MATINS trial dataset (GSE240138),[9] paired pre-therapy and post-therapy tumor biopsies were profiled using GeoMx DSP to obtain spatial transcriptomics profiles of $CD68^+$ and $CD68^-CD31^-$ tumor areas. The GeoMx DSP and original data analysis were previously described.[9] For this study, we reanalyzed the data of patients with RECIST 1.1-defined disease control during bexmarilimab therapy (n=33 biopsy regions; pre-therapy: n=3 patients and 10 regions; post-therapy: n=3 patients and 23 regions). Segment quality control, probe quality control, and region of interest (ROI) filtering were performed using the R packages GeoMx tools (V.3.6.2) and NanoStringNCTools (V.1.10.1) identically as in the original publication. Gene filtering was performed separately for the $CD68^-CD31^-$ (TME) and $CD68^+$ monocyte and macrophage (MoMac, based on deconvolution in the original publication) data by excluding genes that did not exceed both the limit of quantification and a value of 2 in >33.3% of biopsy regions. Filtered, Q3-normalized, and log-transformed

data from patients with disease control were subjected to differential gene expression analysis using a linear mixed model with biopsy type (post vs pre) as a fixed effect and patient ID as a random effect (function: mixedModelDE). DEGs were defined based on $|\log_2\text{FoldChange}|>0.585$ and adjusted p value (Padj, Benjamini-Hochberg) <0.1.

In the Ovarian ascites dataset (GSE222649), ascites cell samples from patients with ovarian cancer were treated ex vivo with bexmarilimab and analyzed by single-cell RNA sequencing (scRNA-seq), as described.[13] MoMacs or total cells from bexmarilimab-responsive ascites samples, defined by *MX1* upregulation in the original publication,[13] were further analyzed for differential gene expression (n=4 patients) with Seurat (V.5.0.3). Genes expressed in >15% (MoMac) or >5% (total) of cells and with an average expression of >0.1 were included in the analysis. DEGs between bexmarilimab-treated and IgG4-treated MoMacs were identified by logistic regression using Patient_ID as a latent variable (Seurat::FindMarkers, bexmarilimab vs IgG4). MoMac DEGs were defined as genes with Padj <0.05, $|\log_2\text{FoldChange}|\geq 0.32$, and upregulated or downregulated in at least three out of four patients ($|\log_2\text{FoldChange}|\geq 0.20$). To mimic the MATINS trial GeoMx DEGs from $CD68^-CD31^-$ areas, we also identified DEGs across all single-cell types. This analysis was performed by identifying and filtering DEGs in each major single-cell cluster (T, B, natural killer cell, dendritic cell, fibroblast, cancer cell, MoMac) as described for the MoMac DEG analysis. To facilitate detection in bulk RNA, we additionally filtered the obtained DEGs: pseudobulk samples were prepared by summarizing counts from all cell types, resulting counts were size factor-normalized with DESeq2 (V.1.42.1), and $|\log_2\text{FoldChange}|$ values were ≥0.32.

Venn diagrams of DEGs were plotted with the R package VennDiagram (V.1.7.3) separately for upregulated and downregulated DEGs from macrophage ($CD68^+$ or MoMacs) and TME ($CD68^-CD31^-$ or all single cells) data.

Patient-derived explant cultures

Culture and bexmarilimab treatment

Breast cancer tumors and adjacent cancer-free tissues were processed at room temperature within 1 hour after surgery. Tissues were cut using scalpels. To capture tissue heterogeneity and avoid sampling-related bias, 6–9 replicate tissue pieces were cut from different tissue areas for each experimental condition. From each selected tissue area, adjacent 1–2 mm^3 pieces were cut and divided across treatment conditions. For ex vivo culture and antibody treatment, two (qPCR) or three (RNA-seq) replicate tissue pieces per well were transferred on a 96-well ultra-low attachment plate (Corning, cat. 7007) containing 200 µL RPMI-1640 (Sigma, cat. 5886), 10% FBS (Sigma, cat. F7524), 1% GlutaMAX (Gibco, cat. 35050-038), 12.8 U/mL penicillin-streptomycin (P/S; Gibco, cat. 15140-122), 20 µg/mL bexmarilimab (FP-1305, Abzena, batches P81902A, 9189203A1, and NBO131P77) or IgG4 isotype control (human IgG4 (S241P/L248E), Abzena, batches 01/171120 and 17528). After incubating the tissues at 37°C and 5% CO_2 for the indicated times, culture media were collected, centrifuged at 4°C at 2,000×g for 5 min, and frozen in aliquots. Tissue pieces were transferred in 1 mL of TRIsure (Bioline, cat. BIO-38032), dissociated in gentleMACS M tubes by running the program RNA.01_01 on a gentleMACS Dissociator (both Miltenyi Biotec, cat. 130-093-235 and 130-093-236), and stored at −70°C until RNA extraction.

Conditioned medium collection and treatment

Tumor or adjacent tissue pieces (two per well, eight replicate wells) were cultured in RPMI supplemented with 10% FBS, 1% GlutaMAX, and P/S for 24 hours as described above. After 24 hours, tissue-conditioned medium was collected from replicate wells and centrifuged at 2,000×g for 10 min at 4°C to remove cells. For cytokine profiling using Bio-Plex, the medium was aliquoted and frozen at −70°C. For ex vivo treatment, freshly collected conditioned medium was used. After conditioned medium collection at 24 hours, adjacent tissue pieces were washed with PBS and treated with 20 µg/mL bexmarilimab or IgG4 in fully supplemented RPMI medium for 1 hour. Then, fresh tumor or adjacent tissue-conditioned medium was added at a ratio of 1:10 to adjacent tissue explant cultures for 48 hours. Finally, the culture medium was collected, centrifuged at 2,000×g at 4°C for 5 min, and frozen for cytokine profiling (Bio-Plex).

Statistical analysis

Statistical tests were performed, and graphs were generated using GraphPad Prism (V.9.2.0 or V.10.0.3) or R (V.4.0.4 or V.4.3.2) software. Data are presented as mean±SD or median±IQR, as indicated in the figure legends alongside n numbers and statistical tests. Parametric and non-parametric statistical tests were selected after determining the data distribution. To compare two independent groups, Student's t-test or Mann-Whitney U-test was used. For comparing paired samples, the paired t-test or Wilcoxon matched-pairs signed-rank test was used. To compare multiple groups, two-way repeated measures analysis of variance followed by Šídák's multiple comparisons test, or Kruskal-Wallis test (function kruskal.test) followed by Dunn's test with Bonferroni correction (package dunn.test) was used. For evaluating equality of variances between groups, Levene's test was used. GeoMx housekeeping gene correlation was evaluated with Pearson's correlation coefficients calculated from unnormalized $\log_2$-transformed counts, and *STAB1* correlation with CD68– area gene expression was evaluated with Spearman's correlation coefficients. A $p<0.05$ was considered statistically significant. The area under the receiver operating characteristic (ROC) curve (AUC) was calculated using the R package pROC (V.1.18.5). The baseline IFNγ cut-off value was determined using ROC analysis with disease control as the endpoint. The cut-off value of 6.25 pg/mL was determined based on the Youden index using five cancer cohorts with high disease control rates in the MATINS trial (cutaneous melanoma, hepatocellular

carcinoma, gastric adenocarcinoma, biliary tract cancer, and ER+breast cancer). Overall survival was analyzed using the Kaplan-Meier method and the log-rank test.

Remaining analysis methods, including RNA sequencing (RNA-seq), quantitative PCR (qPCR), multiplex cytokine profiling, immune landscape analysis, scRNA-seq and digital spatial profiling, have been described in online supplemental file 2.

RESULTS

Breast cancer PDECs recapitulate ex vivo responses to bexmarilimab

Using our previously established PDEC model,[17] we examined which TME properties influence patient sensitivity to bexmarilimab. For this purpose, we first evaluated the ability of our PDEC model to capture clinically observed responses to bexmarilimab therapy and identify markers that can be used to distinguish bexmarilimab-sensitive PDECs. Two published datasets were used to identify bexmarilimab treatment-induced changes in gene expression (figure 1A): (1) a "MATINS trial" dataset of tumor pretreatment and post-treatment biopsies analyzed by spatial transcriptomics and (2) an "Ovarian ascites" dataset of ex vivo treated ascites cells analyzed by scRNA-seq. To identify the core bexmarilimab response associated with treatment benefit and immune activation, DEGs in each dataset were analyzed only from patients with disease control during bexmarilimab therapy or ex vivo observed immune activation, respectively (online supplemental file 4). We identified 16 TME-upregulated and 1 TME-downregulated genes common to both datasets, predominantly comprising genes related to IFN responses (figure 1B). As immune activation following Clever-1 blockade is primarily associated with disruption of MoMac Clever-1,[9 18] we also analyzed DEGs from these cell types and observed 16 upregulated genes common to both datasets, which partially overlapped with the TME-upregulated genes (figure 1C).

Next, the bexmarilimab response gene signature was evaluated using our PDEC model. Breast tumor PDECs were treated with bexmarilimab or isotype control IgG4 for 48 hours, and responses were analyzed by RNA-seq. To focus on genes more consistently changing in breast cancer PDECs, we only selected response genes (either TME-derived or MoMac-derived) that were upregulated in at least three PDECs ($\log_2$FoldChange>0.32): *APOL4*, *CXCL9*, *FCGR1A*, *FGL2*, *GBP5*, *HLA-DOA*, *SERPING1*, and *SLAMF7*. Five out of 13 PDECs showed upregulation in ≥50% of these genes following treatment with an average $\log_2$FoldChange of >0.32 in the upregulated genes (figure 1D and online supplemental figure S1A), and they were categorized as bexmarilimab-responsive. The top genes associated with bexmarilimab-responsive PDECs were *GBP5*, *FCGR1A*, *SERPING1*, *SLAMF7*, and *CXCL9*, with an AUC ≥0.75 (figure 1E and online supplemental figure S2B). These five genes are all IFNγ-stimulated (Interferome v2.0, Hallmark IFNγ M5913),[19 20] with functions in inflammasome activation (*GBP5*),[21] antibody effector functions (*FCGR1A*),[22] complement regulation (*SERPING1*),[23] macrophage activation (*SLAMF7*),[24] and T cell chemotaxis (*CXCL9*).[25] For many of these genes, elevated expression before or on immune checkpoint blockade has been associated with therapeutic responses.[26–28]

To validate that concurrent upregulation of these top five genes characterizes a subgroup of PDECs sensitive to bexmarilimab, a validation set of tumor PDECs (n=24 patients) was treated ex vivo with bexmarilimab or IgG4 for 48 hours (n=5) or 24 hours (n=19), and bexmarilimab response gene expression was measured by qPCR. The upregulation of bexmarilimab response genes was detectable at both time points with similar ranges in relative quantification values (online supplemental figure S1C). Bexmarilimab-induced changes in the five response genes clustered the PDECs into two well-separated groups (figure 1F), characterized by either upregulation (responsive) or downregulation (non-responsive) of the five genes (figure 1G). All five response genes were significantly upregulated in the responsive group, with four genes showing high AUC values (≥0.90) and statistically significant upregulation (figure 1G). In each responsive PDEC, at least four of the five response genes were upregulated (figure 1H), indicating that measuring bexmarilimab-induced upregulation in these five response genes can identify a subset of bexmarilimab-sensitive PDECs. Based on gene expression changes, the proportion of bexmarilimab-sensitive PDECs (9/24, 38%) also matched the proportion of patients with ER+breast cancer achieving disease control during bexmarilimab therapy in the MATINS trial (4/10, 40%).[9] Therefore, our set of top bexmarilimab response genes can be used to identify bexmarilimab-sensitive breast cancer PDECs that exhibit treatment responses similar to those of patients receiving the immunotherapy.

Bexmarilimab stimulates adaptive immunity in responsive tumors and dampens inflammation in resistant tumors

After identifying bexmarilimab-sensitive PDECs, we further explored how bexmarilimab altered gene expression in responsive and non-responsive breast tumors using the PDEC discovery set. Bexmarilimab upregulated proinflammatory pathway-related gene expression (Allograft rejection, Complement, TNFα signaling, IL2 signaling, and Inflammatory response) in responsive tumors, but downregulated IFNα and IFNγ signaling in non-responsive tumors (figure 2A,B). Opposite effects on immune responses were confirmed with a more comprehensive DEG and pathway enrichment analysis (figure 2C–E), which showed activation of immune cell communication and cytokine secretion in responsive tumors (figure 2E), but dampening of chemokine secretion (*CXCL9-11*, *CCL4-5*) and T cell-related gene expression (*CD3E*, *LCK*, *CD28*, T cell receptor signaling) in

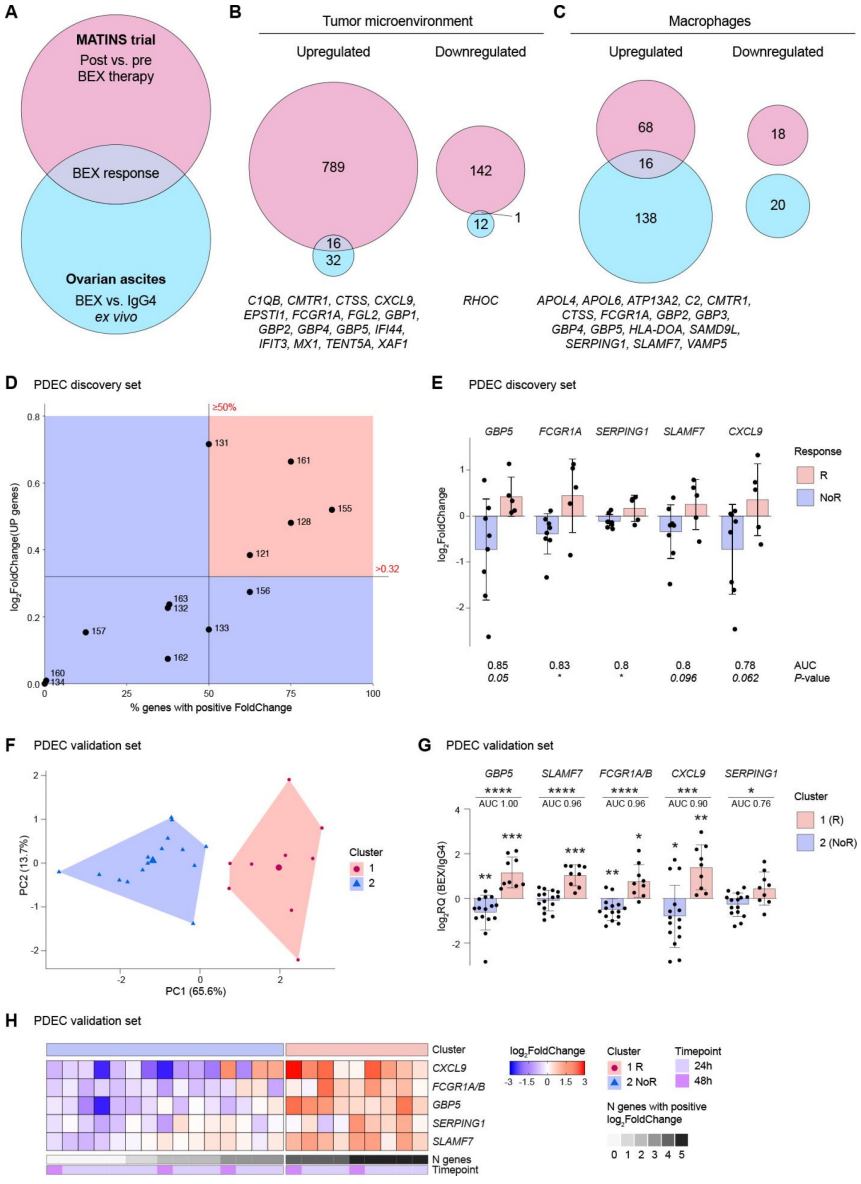

Figure 1 Identification of core bexmarilimab response genes in bexmarilimab-treated patients, patient-derived cells, and tumor explants. (A) Datasets used for bexmarilimab response gene identification: The MATINS trial dataset consists of pre-treatment and post-treatment biopsies from patients with disease control during bexmarilimab therapy (n=3 patients), which was analyzed by GeoMx digital spatial profiling (n=33 biopsy regions). The Ovarian ascites dataset consists of patients with ovarian cancer (n=4) whose ascites cells were responsive to ex vivo bexmarilimab treatment, as analyzed by scRNA-seq. (B–C) Venn diagrams showing genes upregulated or downregulated by bexmarilimab in the MATINS trial (pink) and ovarian ascites (light blue) datasets in the whole TME (B) or macrophages (C). Common DEGs are indicated below the plots. (D) Categorization of breast tumor PDECs (n=13 patients, discovery set) into bexmarilimab responsive (R) and non-responsive (NoR) based on bexmarilimab core response genes identified in (A) and upregulated in at least three tumor PDECs during ex vivo bexmarilimab treatment (*APOL4, CXCL9, FCGR1A, FGL2, GBP5, HLA-DOA, SERPING1, SLAMF7*). Responsive PDECs (red area) were identified based on ≥50% of upregulated genes and >0.32 average log_2FoldChange (BEX/IgG4) in the upregulated (UP) genes. (E) log_2FoldChange (BEX/IgG4) in genes from (D) with AUC ≥0.75 and p<0.1. Points indicate individual patient PDECs (NoR: n=8; R: n=5). Mean±SD, Student's t-test. (F), K-means clustering of breast tumor PDECs (n=24 patients, validation set) into two groups based on log_2FoldChanges (BEX/IgG4) in the top five bexmarilimab response genes identified in (E). Principal component analysis of the measured log_2FoldChanges was used to visualize the clusters. Small points indicate individual patients, and large points indicate cluster centers. (G), log_2FoldChanges (BEX/IgG4) in k-means clusters 1 and 2 and the corresponding AUC values for each gene in the PDEC validation set. Points indicate individual patients. Mean±SD. Cluster deviations from zero were compared using the one-sample t-test, and two clusters were compared using Student's t-test. (H), Heatmap showing bexmarilimab-induced changes in the expression of the top five bexmarilimab response genes separately for each PDEC in the validation set. The columns correspond to individual patients. Annotations indicate k-means clusters, bexmarilimab treatment duration, and number of genes with positive log_2FoldChange. *p<0.05; **p<0.01; ***p<0.001; ****p<0.0001. See also online supplemental figure S1 and file 4. AUC, area under the curve; BEX, bexmarilimab; DEGs, differentially expressed genes; PDEC, patient-derived explant culture; RQ, $2^{-\Delta\Delta CT}$ values from relative quantification.

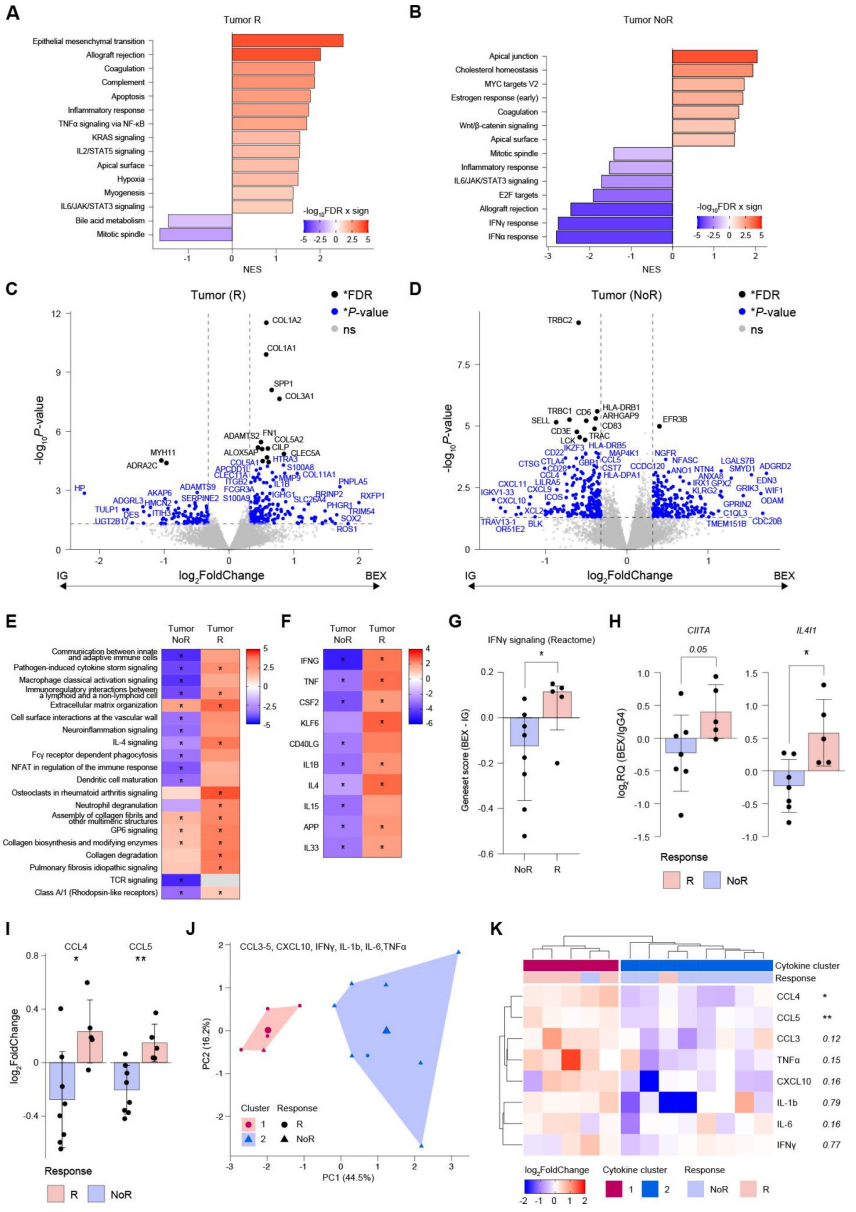

Figure 2 Bexmarilimab activates immunity in sensitive tumors and inhibits inflammation in resistant tumors. (A–B), RNA sequencing of breast cancer patient-derived explant cultures (PDECs) after 48 hours of bexmarilimab or IgG4 treatment. Bar plots show normalized enrichment score (NES) values from hallmark gene set enrichment analysis (GSEA) in bexmarilimab-responsive (R, n=5) (A) and non-responsive (NoR, n=8) (B) tumors. Red color indicates gene set upregulation and blue downregulation by bexmarilimab compared with IgG4-treated tumors. Gene sets with FDR<0.05 are presented. (C–D), Volcano plots of differentially expressed genes (DEGs) in bexmarilimab-responsive (C) and non-responsive (D) tumors. (E–F), Top differentially activated pathways (E) and upstream regulators (F) in bexmarilimab-responsive and non-responsive tumors based on the IPA core analysis of genes from (C–D). Color gradient showing activation z-score with red indicating upregulation. Pathways or regulators with Benjamini-Hochberg-adjusted p values <0.05 are indicated by asterisks. (G), Change in IFNγ signaling scores after bexmarilimab treatment in bexmarilimab-responsive and non-responsive tumors. Mann-Whitney U-test, median±IQR. Points represent individual patient PDECs. (H), PDEC validation set tumors measured for *CIITA* and *IL4I1* expression by qPCR after 24 hours of treatment with bexmarilimab or isotype control IgG4. Points represent individual patient PDECs, mean±SD, Welch's t-test. The R group deviation from 0 was analyzed using the one-sample t-test (*CIITA:* p=0.09; *IL4I1:* p=0.06). (I–K), PDEC supernatant cytokine profiling after 48 hours of bexmarilimab or IgG4 treatment (PDEC discovery set tumors, n=13). Bar plots show cytokines that were upregulated more in bexmarilimab-responsive tumors. Mean±SD, Student's t-test, one-sample t-tests for deviation from 0 (CCL4 R: p=0.09; CCL4 NoR: p=0.06; CCL5 R: p=0.08; CCL5 NoR: p=0.02) (I). Principal component analysis plot showing the k-means clustering of PDECs into two groups based on log_2FoldChanges (BEX/IgG4) in the indicated cytokines (J). Heatmap showing the indicated cytokine log_2FoldChanges, unsupervised clustering of PDECs based on their cytokine profile, annotations for k-means cytokine clusters (1 vs 2), and PDEC RNA-seq response group (R vs NoR). P values for Student's t-test between R and NoR PDECs are shown on the right (K). *P value or FDR<0.05. See also online supplemental figure S1 and file 4. BEX, bexmarilimab; FDR, false discovery rate; IPA, Ingenuity pathway analysis; RQ, $2^{-\Delta\Delta CT}$ values from relative quantification.

non-responsive tumors (figure 2D,E, online supplemental file 4). These changes were predicted to primarily emerge from upstream regulation by IFNγ and TNFα, which would be upregulated in responsive tumors and downregulated in non-responsive tumors (figure 2F). Both of these proinflammatory mediators are associated with the mode of action of bexmarilimab,[9 11] further supporting the relevance of our PDEC model. To confirm opposite regulation by the top upstream regulator IFNγ, we calculated gene set scores for IFNγ signaling and observed significant upregulation in responsive tumors compared with non-responsive tumors (figure 2G). Further, we measured genes induced by IFNγ (*CIITA*) or type I IFNs (*MX1*) and IFN-related negative feedback mechanisms (*IL4I1*, *IDO1*, *CD274*) and observed that *CIITA* (p=0.05) and *IL4I1* (p=0.02) were selectively upregulated in responsive tumors (figure 2H and online supplemental figure S1D).

Because our gene expression analyses identified dual cytokine responses after bexmarilimab treatment, we measured cytokine levels from the PDEC discovery set culture supernatants. After 48 hours of treatment with bexmarilimab, CCL4 and CCL5 were significantly upregulated in bexmarilimab-responsive PDECs (figure 2I). Together with additional cytokines and chemokines previously shown to be induced by bexmarilimab (TNFα, IFNγ, CXCL10),[9 11 13] its parent antibody 3-372 (CCL3),[29] or murine Clever-1 function-blocking antibody mStab1.2 (IL-1β, IL-6),[30] 11 out of 13 PDECs were correctly categorized as responsive or non-responsive based on the cytokine profile alone (figure 2J,K).

In summary, based on our top response genes, bexmarilimab responses in tumor PDECs can be divided into two distinct categories, effectively capturing the key heterogeneity in treatment outcomes. These responses range from immune activation and immune cell recruitment to the suppression of the immune response. This dual effect, depending on bexmarilimab sensitivity, aligns with previous observations in tumor biopsies of patients who either achieve or do not achieve disease control during bexmarilimab immunotherapy.[9] These findings further underscore the translational value of our PDEC model.

Bexmarilimab and anti-PD-(L)1 target opposite TMEs defined by IFN signaling and late-stage activated macrophages

Effective cancer immunotherapy entails recognizing appropriate patients based on their highly heterogeneous TMEs. We searched for TME properties associated with bexmarilimab response by comparing our PDEC discovery set of tumors based on their bexmarilimab sensitivity. Without bexmarilimab treatment, responsive breast cancer PDECs exhibited lower inflammatory gene expression, including IFNα, IFNγ, TNFα, and IL-2 signaling, than non-responsive PDECs (figure 3A). A more comprehensive DEG and pathway analysis confirmed that responsive tumor PDECs showed overall lower activation status in the majority of immune system function-related pathways and their predicted proinflammatory upstream regulators (IFNγ, IL-2, TNFα, BHLHE40) (figure 3B,C, online supplemental figure S2A and file 4). Untreated responsive tumors (without ex vivo culture) also showed a trend toward expressing less IFN-responsive genes, especially the immunosuppressive enzymes IL4I1 and IDO1 induced by prolonged IFN exposure, but high interpatient variation prevented us from making statistical conclusions based on individual genes (online supplemental figure S2B).

We also analyzed whether the response to bexmarilimab was associated with Clever-1 expression, cytokine profile, or tumor histopathological features. Responsive and non-responsive tumors expressed equal Clever-1 mRNA (*STAB1*) levels (online supplemental figure S2C), and cytokine secretomes measured from IgG4-treated tumors varied more between patients than between responsive and non-responsive tumors (data not shown). Although most patient characteristics were equally distributed between the responsive and non-responsive patient groups, non-responsive tumors appeared to more commonly represent ductal carcinoma (p=0.10) (online supplemental table S2), which has fewer protumoral anti-inflammatory TAMs than lobular carcinoma.[31]

Our previous work with ex vivo treated ovarian ascites cells identified a higher abundance of regulatory T (T_{REG}) cells and IL4I1 macrophages in bexmarilimab-resistant samples.[13] We observed a similar trend for more T_{REGs} in non-responsive PDECs by cell type deconvolution (p=0.09) (online supplemental figure S2D) and confirmed a significantly higher IL4I1 macrophage abundance in bexmarilimab-resistant tumors with two different IL4I1 macrophage signatures[7 32] quantified from our RNA-sequenced tumor PDECs (figure 3D). We searched for further differences between responsive and non-responsive PDECs using macrophage subset signatures from three different single-cell atlases and found a higher abundance of IFN-regulated subtypes in non-responsive tumors (online supplemental figure S2E).

Recent studies have established the importance of IL4I1 macrophages, sometimes called late-stage activated macrophages, for cancer prognosis and immune checkpoint inhibitor (ICI) therapy outcome by showing that IL4I1 macrophages are associated with longer survival in colorectal cancer and response to anti-PD-(L)1 therapy in advanced or neoadjuvant-treated breast cancer and human melanoma.[7 32] Therefore, both higher IFN signaling and IL4I1 macrophage abundance before treatment correlate with anti-PD-(L)1 therapy responses in patients with cancer[7 32–35] but were associated with resistance to bexmarilimab treatment in our PDEC model, indicating that bexmarilimab targets immunologically opposite TME types than anti-PD-(L)1 therapy. Although treatment sensitivity showed opposing associations with baseline IFN signaling, both anti-PD-(L)1 and bexmarilimab elicit IFN responses on successful immunotherapy.

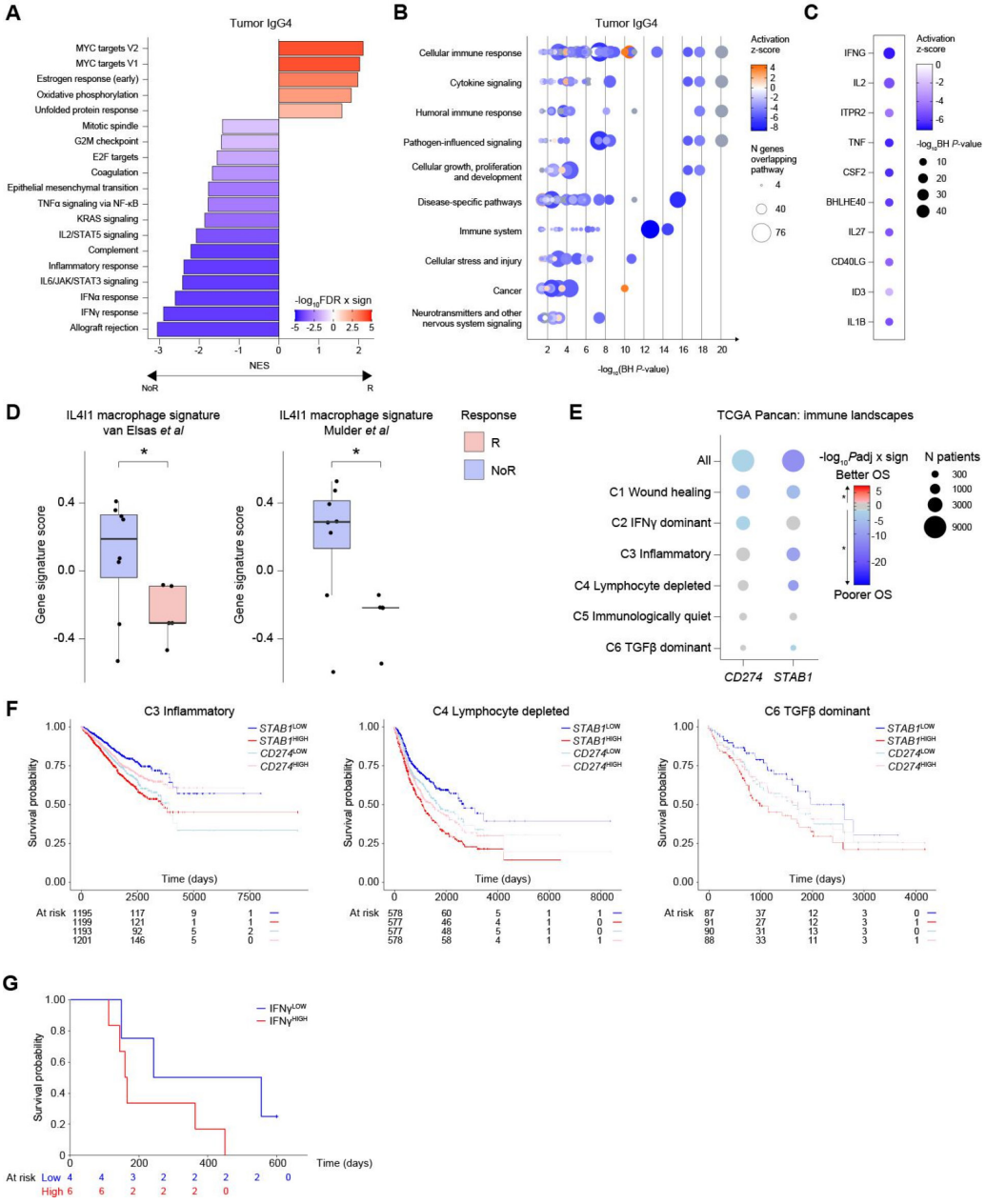

Figure 3 Bexmarilimab-sensitive patient-derived explant cultures (PDECs) have characteristics opposite those of anti-PD-(L)1-sensitive tumors. (A), Gene set enrichment analysis (GSEA) comparing hallmark gene set expression between bexmarilimab-responsive (R, n=5) and non-responsive (NoR, n=8) tumors without bexmarilimab treatment. Bar plots showing the normalized enrichment scores (NES) for gene sets with FDR<0.05 with red color indicating higher expression in bexmarilimab-responsive tumors. (B), Differentially activated pathways between bexmarilimab-responsive and non-responsive tumors (IgG4-treated) based on the IPA core analysis of genes are shown in online supplemental figure S2. Color gradient showing pathway activation z-scores (orange indicates higher and blue indicates lower expression) in bexmarilimab-responsive tumors. Each dot represents a significantly differing pathway (Benjamini-Hochberg (BH)-adjusted p<0.05) belonging to the IPA pathway categories shown on the y-axis. (C), Predicted upstream regulators of the observed gene expression differences between bexmarilimab-responsive and non-responsive tumors based on the IPA core analysis of genes are shown in online supplemental figure S2. Color gradient showing the predicted regulator activation z-scores (blue indicates lower activation) in bexmarilimab-responsive tumors. The top 10 upstream regulators with absolute activation z-scores >2 and BH-adjusted p values <0.05 are presented. (D), IL4I1 macrophage signature scores in bexmarilimab-responsive and non-responsive IgG4-treated tumors. Boxplots show median±IQR. Student's t-test (left) or Mann-Whitney U-test (right) according to data distribution. (E–F), Overall survival based on median *CD274* or *STAB1* expression in TCGA Pancan dataset (n=9,125 primary tumors) is shown separately for each tumor immune landscape subtype. Dot plot colored by log-rank test p values (E) and associated Kaplan-Meier curves (F). (G), Overall survival of patients with ER+ breast cancer treated with bexmarilimab in the MATINS trial. Patients were categorized into two groups based on serum IFNγ levels pretreatment (cut-off 6.25 pg/mL). Log-rank test p=0.14, censored events indicated with |. *P value or FDR<0.05. See also online supplemental figure S2 and table S1. BEX, bexmarilimab; FDR, false discovery rate; IPA, Ingenuity pathway analysis; OS, overall survival; Padj, Benjamini-Hochberg-adjusted p value.

To explore further TME subtypes targeted by bexmarilimab and ICI, we analyzed how the target molecules of these immunotherapies associate with patient survival in different types of tumor immune microenvironments. Thorsson *et al* categorized tumor immune landscapes into six subtypes (wound healing, IFNγ dominant, inflammatory, lymphocyte depleted, immunologically quiet, and TGFβ dominant),[14] and we evaluated overall survival based on *STAB1* and *CD274* (PD-L1) expression using the TCGA Pancan dataset. Although both *STAB1* and *CD274* were associated with poorer overall survival in the whole dataset and wound-healing landscape, *STAB1* was uniquely associated with poorer prognosis in inflammatory, lymphocyte-depleted, and TGFβ-dominant immune landscapes and *CD274* in IFNγ-dominant landscape (figure 3E,F and online supplemental figure S2F,G). *STAB1* also shared similar, but not identical, associations with another macrophage treatment target, *TREM2* (online supplemental figure S2F). We opted to compare *STAB1* survival associations with *CD274*, as other ICI target molecules, including *PDCD1* (PD-1) and *CTLA4*, are expressed on T cells and their association with survival would be confounded by their positive correlation with overall lymphocyte count, as suggested by our analyses (online supplemental figure S2F). The observed differences in association with overall survival further point out that bexmarilimab-targeted and PD-(L)1-targeted therapies would best benefit complementary patient populations. With *CD274* correlated with poorer survival in IFNγ-dominant TME and high pre-treatment IFN signaling associated with anti-PD-(L)1 responses, we analyzed whether low serum IFNγ levels pre-treatment could predict response to bexmarilimab therapy. In support of our PDEC discoveries, we observed a trend toward longer overall survival in the MATINS trial among patients with ER+ breast cancer and low IFNγ pretreatment levels (figure 3G, p=0.14, online supplemental table S1).

In conclusion, bexmarilimab-sensitive tumors have lower baseline levels of immune activation, and resistance to bexmarilimab is particularly associated with late-stage activated IL4I1 macrophages and IFN signaling. These features are opposite to those of tumors most likely to benefit from currently approved anti-PD-(L)1 therapies.

Bexmarilimab elicits B cell responses in adjacent cancer-free breast tissue regardless of tumor bexmarilimab sensitivity

Under homeostasis, healthy tissues lack chronic IFN signaling and late-stage activated macrophages, potentially allowing bexmarilimab to activate the immune system. Moreover, healthy tissues do not possess the immunostimulatory properties of the TME, such as danger signals and tumor antigens. Expectedly, we observed lower abundancies of immune cells, particularly memory cell types, in adjacent cancer-free tissues compared with the corresponding tumors (online supplemental figure S3A). To understand how bexmarilimab therapy affects cancer-free tissues, we treated both tumors and adjacent, pathologically verified, healthy tissues of the same patients with bexmarilimab for 48 hours and compared subsequent immune responses by RNA-seq.

Patients with bexmarilimab-responsive tumors generally showed similar upregulation of core bexmarilimab response genes in both adjacent and tumor PDECs (figure 4A,B). However, in non-responsive patients, bexmarilimab was able to induce core response genes only in adjacent cancer-free PDECs (figure 4A,B). Completely opposite responses to bexmarilimab were observed in non-responsive patient tumors and cancer-free tissues, as IFNα, IFNγ, allograft rejection, and inflammatory response gene sets were upregulated in cancer-free tissues and downregulated in tumors after bexmarilimab treatment (figure 2B and online supplemental figure S3B). Overall, our DEG and pathway analyses showed that adjacent tissues of both bexmarilimab-sensitive and bexmarilimab-resistant PDECs respond to bexmarilimab treatment in a rather similar manner as responsive tumor PDECs (figure 4C–F and online supplemental file 4), with upregulation of several immune-related pathways (immune cell communication, phagocytosis, Fc-receptor signaling), mediators (IFNγ, TNF), and IFNγ signaling (figure 4E–G). As a distinctive feature, adjacent tissues from both responsive and non-responsive PDECs showed upregulation of several immunoglobulin genes (figure 4C,D and online supplemental file 4) and B cell receptor signaling, which was not observed in tumor tissues (figure 4E). Furthermore, on comparing cytokine secretion between treated tissues, we unexpectedly observed bexmarilimab-induced upregulation of proinflammatory cytokines and chemokines only in responsive tumors and not in cancer-free tissues (figure 4H–J), despite their similar responses at the gene expression level.

Based on these findings, we demonstrate that adjacent cancer-free tissues respond to bexmarilimab therapy primarily by lowering self-tolerance and consequently promoting B cell activation. However, due to the lack of an immunostimulatory TME, they have a lower capacity to produce immunostimulatory mediators. Notably, the bexmarilimab responses of cancer-free tissues were not dependent on the bexmarilimab sensitivity of the corresponding tumor. Therefore, TME-intrinsic factors appear to not only regulate bexmarilimab resistance but also boost bexmarilimab-induced immune activation.

Clever-1+ macrophages in tumors and cancer-free tissues exhibit different ontogeny

Our analyses revealed three types of responses to bexmarilimab, depending on the type of treated tissue and TME. Adjacent cancer-free tissues exhibited weaker inflammatory responses with pronounced B cell activation, whereas responses in tumors depended on the existing inflammatory status, resulting in either moderate bexmarilimab-induced immune activation or dampening of the ongoing immune response. We, therefore, sought to understand how local tissue microenvironments, together with macrophage-related features, such

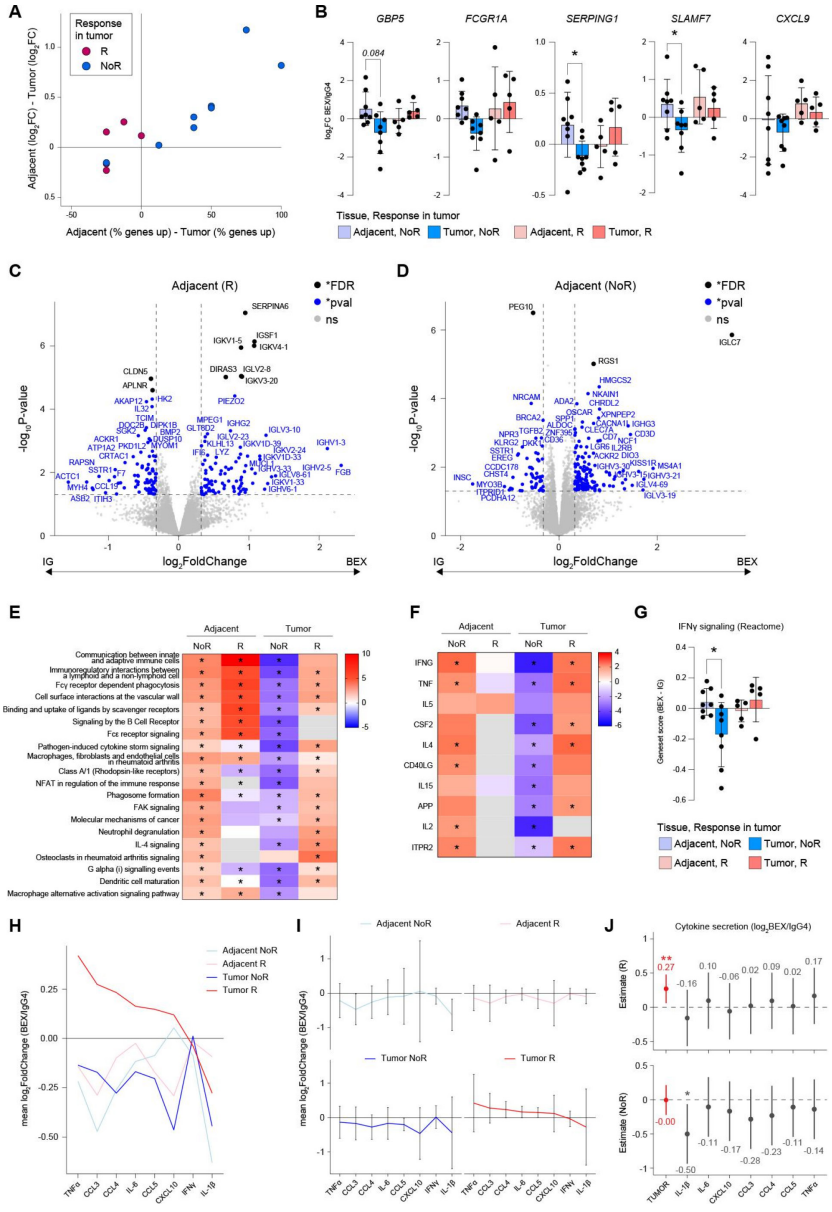

Figure 4 Adjacent cancer-free tissues are activated by bexmarilimab regardless of bexmarilimab sensitivity in the corresponding tumor. (A), PDEC-detectable bexmarilimab response genes (*APOL4, CXCL9, FCGR1A, FGL2, GBP5, HLA-DOA, SERPING1, SLAMF7*) were measured in tumor and adjacent cancer-free PDECs after 48 hours of bexmarilimab treatment by RNA-seq. The bi-plot shows how bexmarilimab upregulates response genes in adjacent cancer-free tissues compared with corresponding tumors (positive values indicate better responses in adjacent cancer-free tissues). The x-axis and y-axis show changes in the expression of upregulated response genes and upregulated gene $\log_2$FoldChange, respectively. (B), Bar plots show $\log_2$FoldChanges in the top five bexmarilimab response genes (validated in figure 1G) separately in tumor and adjacent cancer-free tissue PDECs of bexmarilimab-responsive (R, n=5) and non-responsive (NoR, n=8) patients. Mean±SD, two-way repeated measures ANOVA, followed by Šídák's multiple comparisons test. (C–D), Volcano plots of DEGs in adjacent cancer-free tissues of patients with bexmarilimab-responsive (C) and non-responsive (D) tumors. (E–F), Top differentially activated pathways (E) and upstream regulators (F) in bexmarilimab-responsive and non-responsive tumors and corresponding adjacent cancer-free tissues based on IPA core analyses of genes from (C–D) and figure 2C,D. Color gradient showing activation z-scores (red indicates upregulation). Pathways or regulators with Benjamini-Hochberg-adjusted p values <0.05 are indicated by asterisks. (G), Change in IFNγ signaling scores after bexmarilimab treatment in bexmarilimab-responsive and non-responsive tumors and corresponding adjacent cancer-free tissues. Two-way repeated measures ANOVA, followed by Šídák's multiple comparisons test, mean±SD. Points represent individual patients. (H–I) Line plots showing $\log_2$FoldChanges in PDEC supernatant cytokine levels separately in adjacent cancer-free tissues and tumors of bexmarilimab-responsive (n=5) and bexmarilimab-non-responsive (n=8) patients. Mean (H), mean±SD (I). (J), The effect of tissue type (tumor vs adjacent) and indicated cytokines on $\log_2$FoldChange (BEX/IgG4) in PDEC cytokine secretion was calculated from data in (I). The y-axis shows estimates and 95% CIs from a linear mixed model fitted for bexmarilimab-responsive (R, above) and non-responsive (NoR, below) patients. *p value or FDR<0.05. See also online supplemental figure S3 and file 4. ANOVA, analysis of variance; BEX, bexmarilimab; FDR, false discovery rate; IPA, Ingenuity pathway analysis; PDEC, patient-derived explant culture.

as ontogeny, phenotype, and localization, could regulate different responses to bexmarilimab.

We compared Clever-1+ macrophage ontogeny and phenotypes between tumor and adjacent cancer-free tissues of five patients with treatment-naïve breast cancer by scRNA-seq (figure 5A, online supplemental figure S4A–E). MoMac clustering revealed markedly higher transcriptional heterogeneity among TAMs than adjacent tissue macrophages, as TAMs from different patients formed their own clusters that positioned based on breast cancer subtype (figure 5A). The range of Clever-1 expression appeared higher in adjacent tissues in a patient-specific manner, whereas the overall proportion of Clever-1 macrophages remained consistent between adjacent and tumor tissues (figure 5B). Other Clever-1-expressing cell populations had either significantly lower expression levels (blood endothelial cells) or were less abundant in tumors (lymphatic endothelial cells) (online supplemental figure S4F–G).

To investigate the ontogeny of Clever-1+ macrophages, we evaluated the expression of marker genes previously associated with breast tissue-resident (*FOLR2, LYVE1, MRC1*) and monocyte-derived (*TREM2, SPP1, CADM1*) macrophages.[36] Only Clever-1+ TAMs expressed significant amounts of monocyte-derived macrophage markers, whereas Clever-1+ adjacent tissue macrophages expressed tissue-resident macrophage markers more strongly than Clever-1+ TAMs (figure 5C and online supplemental figure S4H). We also mapped our scRNA-seq MoMacs to a cross-tissue atlas of human monocytes and macrophages[5] (figure 5D). Both tissues showed a large proportion of monocytes, but Clever-1+ adjacent tissue MoMacs were enriched with HES1 tissue-resident macrophages, which were observed to a much lower extent among Clever-1-negative adjacent tissue macrophages or TAMs (figure 5E,F, online supplemental figure S4I). In tumors, Clever-1 was found on immunosuppressive TAMs, which coexpressed IL4I1 (#6) or TREM2 (#3), and dendritic cell-like macrophages (#7), all of which have been described as monocyte-derived populations (figure 5E).[5]

To inspect Clever-1+ macrophage phenotypes more closely, we identified DEGs between Clever-1+ TAMs and Clever-1+ adjacent tissue macrophages (online supplemental file 4 and figure 5G). Clever-1+ TAMs expressed higher levels of apolipoproteins (*APOE, APOC1*) and major histocompatibility complex molecules (*HLA-A, HLA-B, HLA-C, HLA-DRB1, B2M*) (figure 5H) and showed higher levels of IFN signaling, antigen presentation, and other pathways associated with immune activation (figure 5I) compared with adjacent tissue Clever-1+ MoMacs. These gene signatures align well with formerly identified lipid-associated (TREM2+) and IFN-primed (IL4I1+) TAM phenotypes,[4 5] and they were predicted to stem from the upstream regulators IFNγ, BHLHE40, IRF7, TGFβ, and HRG (figure 5I). Of note, these reported differences characterize macrophage populations targeted by bexmarilimab, but may not exclusively associate with Clever-1+ MoMacs in these tissues.

In short, our scRNA-seq analyses collectively show that Clever-1+ TAMs differ from Clever-1+ adjacent tissue macrophages both in their ontogeny (monocyte-derived vs tissue-resident) and more activated phenotype, which likely results from interactions with the surrounding TME that can potentially support both immunosuppressive (TGFβ, apolipoproteins) and immunostimulatory (IFNγ, antigen presentation) phenotypic features.

Clever-1+ TAMs and healthy tissue macrophages reside in T cell-infiltrated and B cell-infiltrated tissue niches, respectively

To gain information on Clever-1-expressing macrophage localization, we performed spatial transcriptomics profiling of tumor and adjacent cancer-free tissue sections from 10 patients with breast cancer and analyzed gene expression from ROIs segmented into CD68+ and CD68− areas (figure 6A). Patients with successful CD68 staining and RNA probe collection (n=8 tumor; n=7 adjacent tissue) and their CD68+ and CD68− segments passing quality control (n=77 tumor; n=66 adjacent tissue areas) were used in downstream analyses. Expression data normalization removed the variation in the overall count distribution between ROIs and diminished the positive correlation of gene expression with the ROI nuclei count, surface area, and background signal, especially in the CD68− area (online supplemental figure S5). Based on dimensionality reduction of all CD68+ and CD68− segments, differences in gene expression were more strongly related to tissue type than to patient or segment type (figure 6B).

We first identified different types of tumors and adjacent tissue niches based on CD68− area gene expression. Using canonical cell-type marker genes for lymphocytes (*CD3E, CD4, CD8A, MS4A1, FOXP3*), myeloid (*CD68, CD163, ITGAX*), cytotoxic (*NKG7*), epithelial (*KRT, EPCAM*), and endothelial (*PECAM1*) cells, tumor and adjacent tissue regions were clustered into six types of tissue niches (figure 6C,D). Both tissue types had regions that were predominantly infiltrated with T_{REGs}, B cells, epithelial cells, or non-regulatory T cells. In addition, tumors had regions with myeloid and CD4+ T cell enrichment, whereas adjacent tissues showed a CD4+ T cell cluster lacking other immune cell types (figure 6C–F). The highest immune cell infiltration was observed in T cell-enriched and T_{REG}-enriched tumor areas, whereas T_{REG}-infiltrated areas in adjacent cancer-free tissues had lower CD45 expression (*PTPRC*, figure 6E,F). Clever-1 expression in CD68+ areas was highest within tumors in immune cell-infiltrated tissue niches, including T_{REGs}, B cell, and myeloid cell regions (figure 6G), whereas MoMac Clever-1 was found on B cell-infiltrated regions in adjacent tissues (figure 6G,H). In contrast to tumors, adjacent tissue niches rich with T_{REGs} showed low levels of Clever-1 expression.

As these findings suggested different associations between MoMac Clever-1 and lymphocyte infiltration depending on tissue type, we evaluated the CD68+ area Clever-1 correlation with leukocytes (*PTPRC*), T cells

Figure 5 Clever-1+ TAMs are monocyte-derived, whereas Clever-1+ adjacent tissue macrophages are resident macrophages with a less activated phenotype. (A) Clustering scRNA-sequenced MoMacs from paired breast cancer tumors and adjacent cancer-free tissues (n=2,809 cells; n=5 patients). UMAP plots are colored according to MoMac cluster, tissue type, or patient ID. (B), Clever-1 mRNA (*STAB1*) expression in adjacent and tumor tissue MoMacs. UMAP plot from (A) colored according to *STAB1* expression (left). Bar plots showing average *STAB1* expression (non-log-scale) or proportion of *STAB1*-expressing MoMacs in each patient (n=5) (right). Median±IQR, Wilcoxon matched-pairs signed rank test. (C), Violin plots of breast tissue-resident and monocyte-derived macrophage marker genes show log-normalized expression levels of *STAB1*+ MoMacs from adjacent tissue (n=405 cells) and tumor tissue (n=902 cells). (D), Mapping of MoMacs from adjacent and tumor tissues to MoMac-VERSE, a human monocyte and macrophage single-cell atlas. Mapped *STAB1*+ MoMacs are highlighted on top of the original MoMac-VERSE UMAP plot and colored according to tissue type (left) or predicted MoMac-VERSE cell type (right). (E), Proportions of predicted MoMac-VERSE cell types among *STAB1*+ and *STAB1*- MoMacs in adjacent and tumor tissue. (F), Percentage of HES1 macrophages among *STAB*1+ and *STAB1*- adjacent and tumor tissue MoMacs. Bars indicate the mean and lines of individual patients. One-way repeated measures ANOVA followed by Šídák's multiple comparisons test (comparisons: *STAB1*+ vs *STAB1*– in adjacent and tumor, *STAB1*+ tumor vs *STAB1*+ adjacent, and *STAB1*– tumor vs *STAB1*– adjacent). (G), DEGs between *STAB1*+ TAMs and *STAB1*+ adjacent tissue macrophages were analyzed separately for each patient with breast cancer. Venn diagrams for genes upregulated in the tumor (top) and adjacent cancer-free tissue (bottom) are presented alongside patient numbers introduced in UMAP plots of panel (A). A patient with HER2+ breast cancer with <5 DEGs was excluded. (H), Expression levels of the top *STAB1*+ tumor and *STAB1*+ adjacent MoMac DEGs from (G). Heatmap showing the expression levels of single MoMacs (n subsetted to ≤100 cells per sample) separately for each patient. (I–J), Top differentially activated pathways (I) and upstream regulators (J) in *STAB1*+ tumor MoMacs compared with *STAB1*+ adjacent tissue MoMacs based on IPA core analyses of DEGs from (G). Color gradient showing activation z-scores (red indicates upregulation in tumor MoMacs and blue indicates upregulation in adjacent MoMacs). Pathways or regulators with *Padj*<0.05 are indicated by asterisks. *p<0.05; ns, not significant. See also online supplemental figure S4 and file 4. IPA, Ingenuity pathway analysis; Lum A, luminal A breast cancer; Lum B, luminal B breast cancer; TNBC, triple-negative breast cancer; UMAP, uniform malifold approximation and projection.

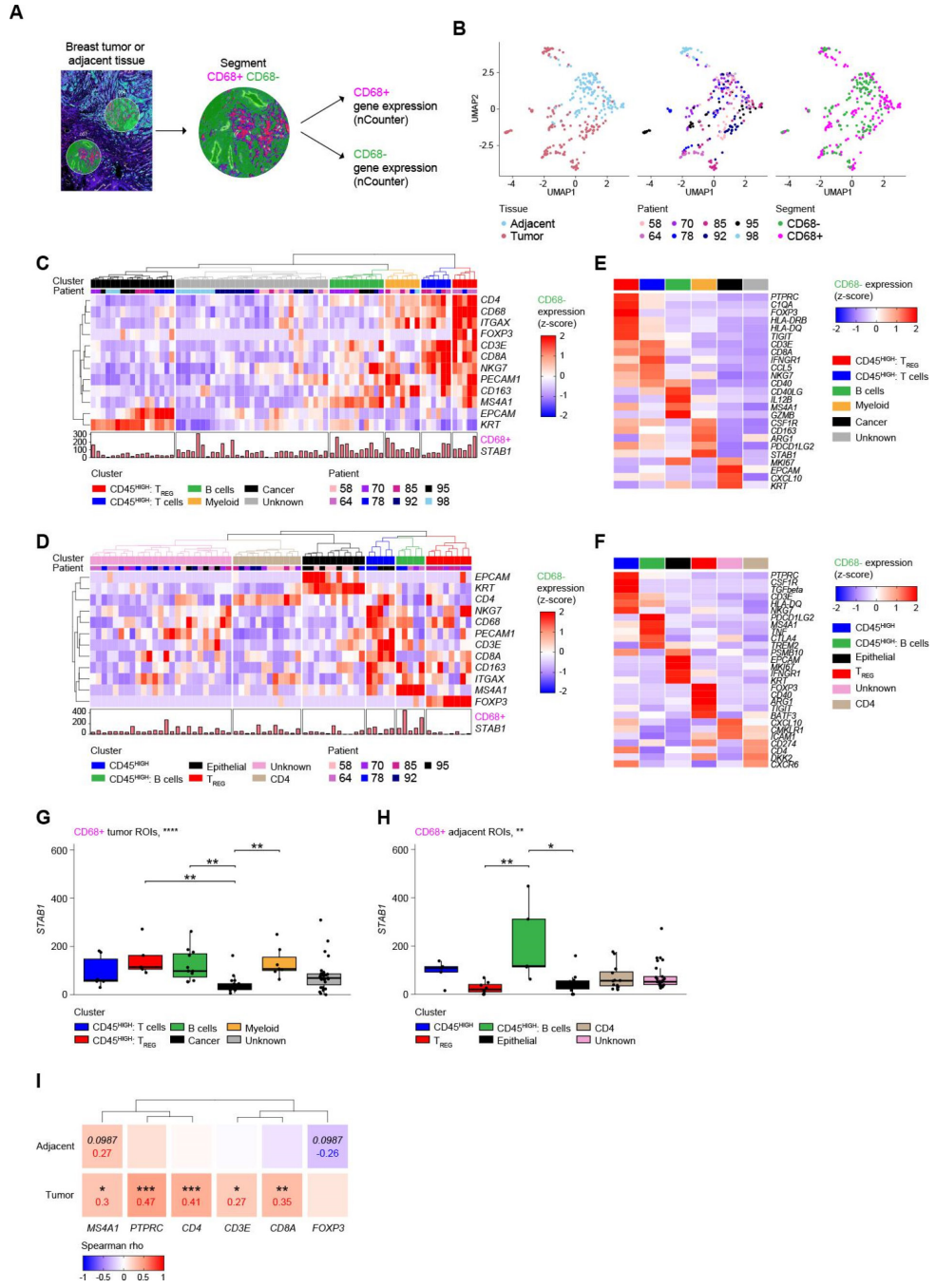

Figure 6 Clever-1+ macrophages reside in B cell-rich healthy tissue niches and immune-infiltrated tumor tissue niches. (A), GeoMx digital spatial profiling of adjacent cancer-free and breast cancer tumor tissue sections (n=8 patients; n=12 ROIs per section). Illustration showing morphological staining for CD68 (magenta), pancytokeratin (cyan), CD31 (yellow), and nuclei (blue) with two ROIs and ROI segmentation into CD68+ and CD68– areas for subsequent separate gene expression profiling with nCounter probes. (B), UMAP dimensionality reduction of the CD68+ and CD68– area gene expression profiles of all ROIs passing quality control (n=77 tumor ROIs; n=66 adjacent tissue ROIs). Scatter plots are colored according to tissue type, patient, or segment type. (C–D) Identification of tissue niches in tumor and adjacent cancer-free tissues based on CD68– segment gene expression. Unsupervised hierarchical clustering of tumor tissue ROIs (C) and adjacent tissue ROIs (D) based on CD68– segment gene expression of the indicated cell-type markers. Each heatmap column represents a single ROI with Clever-1 expression (*STAB1*) in the corresponding CD68+ segment. (E–F), Median expression of CD45 (*PTPRC*) and the top five cluster marker genes (log_2FoldChange (cluster vs other clusters) >1) were plotted as heatmaps separately for tumor (E) and adjacent tissue (F) clusters. (G–H), Clever-1 expression (*STAB1*) in the CD68+ region of the identified tumor (G) and adjacent tissue (H) niches. Each point corresponds to a single ROI, and boxplots show median±IQR. Kruskal-Wallis test followed by Dunn's test. (I), Spearman correlation between CD68+ region Clever-1 expression and indicated gene expression in CD68- area. Adjusted p values and Spearman correlation coefficients for correlations with Padj<0.1. *P or Padj<0.05; **P or Padj<0.01; ***P or Padj<0.001; ****P or Padj<0.0001. See also online supplemental figure S5. PCK, pancytokeratin; ROI, region of interest; UMAP, uniform malifold approximation and projection.

(*CD3E*), CD8+ and CD4+ T cells (*CD8A, CD4*), T_{REG} (*FOXP3*), and B cells (*MS4A1*). In tumors, a significant positive correlation was observed between MoMac Clever-1 and all lymphocyte markers, except *FOXP3* (figure 6I). In adjacent tissues, however, only B cells showed a positive correlation with MoMac Clever-1 expression (p=0.026, Padj=0.099), and we observed a negative trend with *FOXP3* (figure 6I, p=0.033, Padj=0.099). Close localization with B cells or T cells in adjacent and tumor tissues, respectively, would allow Clever-1+ MoMacs to regulate the functions of these lymphocyte subsets and may explain the B cell activation predominantly observed in cancer-free tissues following bexmarilimab treatment.

Tumor secretomes alter bexmarilimab response in cancer-free tissues

Having observed different macrophage phenotypes, ontogeny, and localization between adjacent and tumor tissues, we next wondered whether these characteristics determine the tissue's sensitivity to bexmarilimab or whether macrophage plasticity allows modification of subsequent responses. As macrophages adapt to changes in their environment,[37–39] we hypothesized that altering the local tissue environment would alter PDEC sensitivity to bexmarilimab. To test this hypothesis, we collected tumor and adjacent tissue-conditioned media and treated the same patient's adjacent tissue with bexmarilimab in either adjacent or tumor-conditioned medium (figure 7A). In essence, such treatment transfers the soluble TME into cancer-free tissue that normally exhibits low inflammatory activation in response to bexmarilimab regardless of the patient's bexmarilimab sensitivity.

Surprisingly, bexmarilimab treatment of adjacent tissue exposed to tumor-conditioned medium highly altered its cytokine profile and created two types of responses, either cytokine downregulation or upregulation, which was mostly dependent on the known bexmarilimab sensitivity of the corresponding tumor (figure 7B,C). In particular, cytokines related to immune cell recruitment (CCL2-5, CXCL10) were upregulated more in adjacent tissues treated with bexmarilimab and tumor-conditioned medium (figure 7B,C). These results have two important implications: First, bexmarilimab responses are not restricted by macrophage ontogeny or tissue localization, as changes in the microenvironment allow for different responses. Second, the tumor secretome contains factors that regulate bexmarilimab sensitivity because the transfer of the secretome highly mimicked the patterns of bexmarilimab sensitivity in tumor tissues.

Elucidation of the tumor secretome components responsible for such differential responses was not possible based on cytokine measurements alone, as adjacent and tumor-conditioned media added to the tissue cultures contained similar levels of most cytokines, with the exception of CXCL10 and IL-1ra (figure 7D), and the levels of these two cytokines did not significantly differ between patients showing lower or higher cytokine secretion (figure 7E; adjacent: cluster 1 vs cluster 2; tumor: cluster 1 vs cluster 2).

Based on these results, the proinflammatory activation of MoMacs and related cytokine secretion after bexmarilimab treatment requires a component inherently present in the soluble TME, as well as the simultaneous absence of TME-related factors that promote resistance to bexmarilimab, such as IFN signaling.

DISCUSSION

Growing evidence highlights the clinical potential of selecting treatments through ex vivo profiling, a strategy which allows for a more personalized approach to cancer therapy. Studies have demonstrated that tailoring treatments based on such functional data can improve clinical outcomes by identifying the most effective drugs for individual patients while sparing them from unnecessary toxicity associated with ineffective therapies.[40 41] Moreover, ex vivo profiling can guide combination therapy strategies, address intratumoral heterogeneity, and overcome drug resistance mechanisms. In solid tumors, patient-derived explants provide a powerful platform for revealing drug-induced immune modulation[42] and the mechanisms of response to ICIs.[15 16]

We used our previously established breast cancer explant model and generated clinically actionable insights. We discovered that sensitivity to macrophage reprogramming therapy (bexmarilimab) is regulated by different aspects of local tissue and tumor microenvironments. As shown by a recent phase I/II clinical trial across 10 solid tumor types, bexmarilimab effectively promoted macrophage reprogramming in 30%–40% of patients with refractory tumors and in those considered to be immunologically cold.[9] Our results now indicate that bexmarilimab efficacy is TME dependent and varies according to neighboring cells, the cytokine milieu, and secreted tumor components that enable the therapeutic potential of bexmarilimab. These findings underscore the complexities of targeting macrophages within diverse TMEs, emphasizing the need for careful patient selection when developing macrophage-focused therapeutics.

Bexmarilimab sensitivity in tumors was determined by the level of prior immune system activation, with sensitive tumor PDECs being immunologically quieter. In particular, high IFN signaling and late-stage activated macrophage abundance were associated with bexmarilimab resistance. In sensitive tumor PDECs, bexmarilimab treatment engaged TAMs and T cells in beneficial cooperation via induced chemokine secretion (CXCL9, CCL4, CCL5) and IFNs, which has been shown to improve patient survival and crucially promote T cell-based immunotherapy responses.[25 27 32 43] Interestingly, bexmarilimab treatment for resistant tumor PDECs actually dampened the existing high IFN signaling. Exploring the numerous feedback mechanisms and epigenetic changes imposed by pre-exposure to IFNs in macrophages[44] may reveal how prior chronic IFN stimulus leads to altered

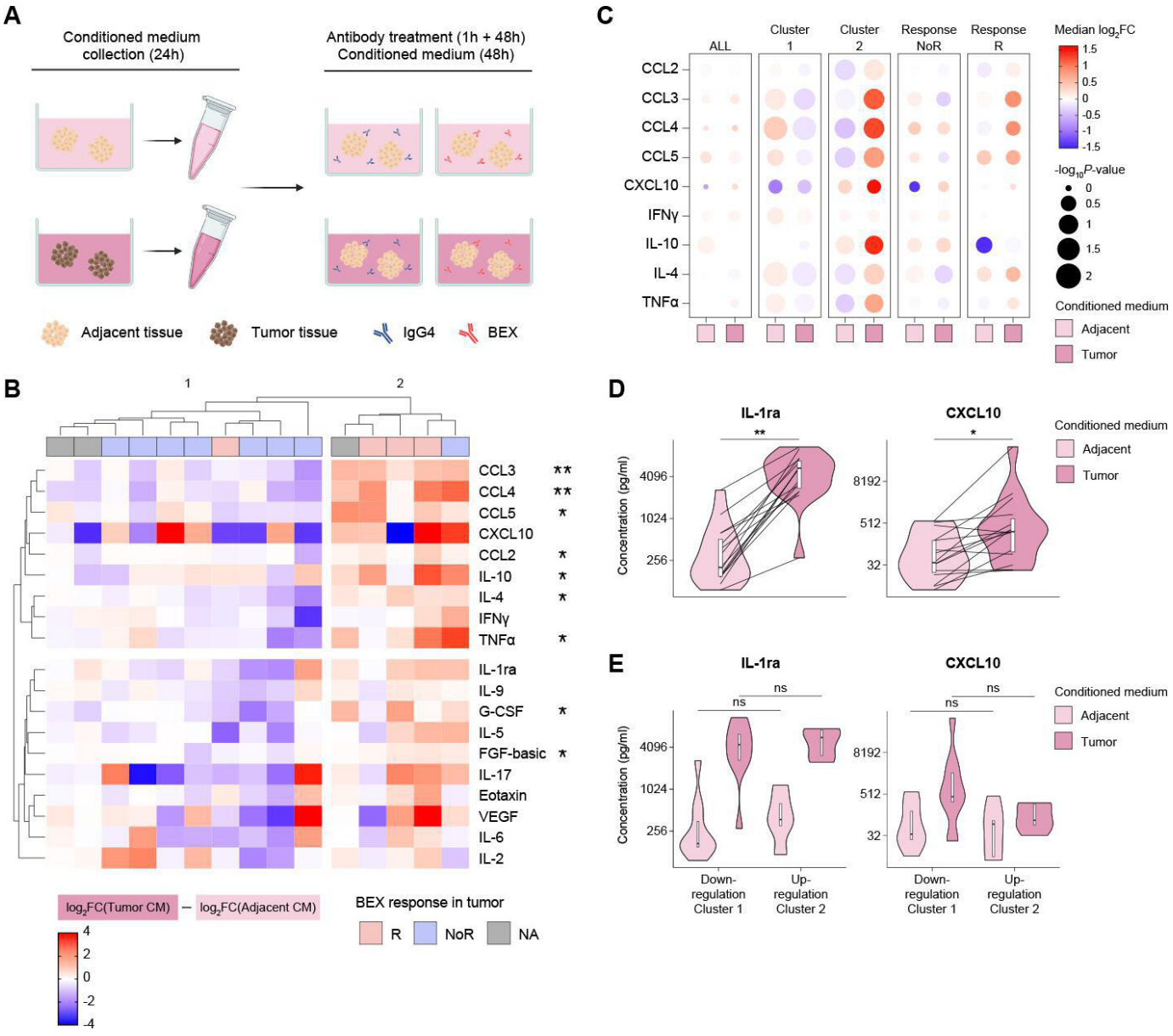

Figure 7 Tumor secretome dampens or strengthens bexmarilimab responses in cancer-free tissues, depending on the bexmarilimab sensitivity of the tumor. (A) A schematic showing adjacent tissue-conditioned and tumor tissue-conditioned media collection and subsequent treatment of the same patient's adjacent tissue with the indicated antibodies and collected conditioned media. Illustration created using BioRender. (B), Cytokine profiling of adjacent tissue culture supernatants after 48 hours of treatment with antibodies (BEX or IgG4) and adjacent or tumor tissue-conditioned medium. Unsupervised hierarchical clustering of adjacent tissues (n=15 patients) based on differences in log_2FC values (log_2FoldChange BEX/IgG4) between tumor-conditioned and adjacent-conditioned media (log_2FoldChange in tumor media – log_2FoldChange in adjacent media). Red color indicates stronger BEX-induced cytokine secretion in the tumor medium. Student's t-test for differences between clusters 1 and 2. (C), Underlying log_2FoldChange values (BEX/IgG4) in adjacent-conditioned and tumor-conditioned media from (B) are shown separately in all patients (n=15), patient clusters 1 and 2 (from B), and bexmarilimab-responsive (R, n=4) and non-responsive (NoR, n=8) patients. Point color indicates median log_2FoldChange in each group, and point size is relative to $-log_{10}$p values from Wilcoxon matched-pairs signed rank (tumor vs adjacent). (D–E) Cytokine concentrations in the collected conditioned medium (24 hours) prior to its addition to antibody-treated adjacent tissues. The concentrations between adjacent-conditioned and tumor-conditioned media were compared using the Wilcoxon matched-pairs signed rank test (n=15), and cytokines with Padj<0.05 are presented (D). For significant cytokines from (D), the conditioned media of cluster 1 and cluster 2 patients were further compared using the Mann-Whitney U-test (E). Boxplots show median±IQR. *P or Padj<0.05; **P or Padj<0.01; ns, not significant. BEX, bexmarilimab; CM, conditioned medium.

signaling on Clever-1 targeting. The clinical implications of such dampening in IFN signaling in non-responsive tumors remain to be investigated. Although acute IFN responses support antitumor immunity, sustained IFN signaling can fuel resistance to cancer immunotherapy, suppressing antitumor T cell responses via protumoral

immune regulatory networks and supporting cancer growth.[45 46] Thus, bexmarilimab could improve exhausted T cell responses in this context.

While our short-term treatment of PDECs limited our ability to draw conclusions about long-term immunological effects or clinical benefits, similar proinflammatory activation within MATINS trial patient tumors was associated with disease stabilization.[9] However, some elevated pathways in responsive tumors, such as IL-1β or IL-4, can promote tumor-sustaining chronic inflammation, depending on signaling strength and duration.[47] Nevertheless, similar elevated IL-4 secretion was observed in PDECs of patients responding to anti-PD-1 therapy.[16]

We extended our studies to cancer-free tissues and observed weaker B cell-dominated immune responses that were not dependent on bexmarilimab sensitivity in tumor PDECs. Our analyses identified an alternative immune cell activation route that could support the therapeutic efficacy of bexmarilimab via B cell functions or, to some degree, also facilitate treatment-emergent autoimmune reactions characteristic of cancer immunotherapy.[48 49] The B cell activation observed in cancer-free tissues is supported by previous studies showing that Clever-1 knockout mice have abnormally high antibody levels under resting conditions and enhanced humoral immune responses after immunizing with protein and carbohydrate antigens. Mechanistically, enhanced secretion of proinflammatory cytokines, including TNFα, by monocytes lacking Clever-1 stimulated stronger IgM production in cocultured B cells.[50] In addition, patients treated with bexmarilimab showed increased numbers of circulating B cells, indicating enhanced B cell recruitment into tumors.[9 12]

Bexmarilimab efficacy was promoted by transferring responsive tumor-conditioned media onto cancer-free tissue. Although this supports our observations that treatment response is modulated by the TME, it is unclear how the TME should be manipulated to sensitize bexmarilimab-resistant tumors to treatment. Some examples include pretreatment with corticosteroids or inhibitors of IFN signaling to expand patient populations eligible for bexmarilimab therapy. Despite this, effective patient selection is essential for optimizing therapeutic outcomes and could be explored by identifying TME features predictive of ICI therapeutic efficacy and refining selection criteria accordingly.

Acknowledgements We thank Teija Kanasuo, Mari Parsama, Maritta Pohjansalo, and Sari Mäki for their excellent technical assistance. scRNA-seq was performed by Single Cell Omics Core at the Turku Bioscience Centre and Finnish Functional Genomics Centre, supported by the University of Turku, Åbo Akademi University, and Biocenter Finland. We also thank all the patients who participated in the study. Faron Pharmaceuticals sponsored the MATINS clinical study.

Contributors JHR, RV, and MH designed the study. JHR and RV optimized ex vivo culture conditions. JHR and RT treated the explants. ATak prepared samples for scRNA-seq. JHR, RT, and CH collected the data. JHR analyzed and visualized the data. PB collected tissue samples and performed histopathological examinations. IK and ATam recruited patients with breast cancer. JHR and MH interpreted the data. JHR wrote the first draft of the manuscript. All authors have reviewed the manuscript and approved its final version. MH is the guarantor of this study.

Funding This study was funded by the Research Council of Finland, Sigrid Jusélius Foundation, Business Finland (all to MH), Finnish Cancer Foundation (MH and JHR), Orion Research Foundation, Paulo Foundation, Ida Montin Foundation, and Emil Aaltonen Foundation (JHR)

Competing interests ATam and MH hold shares of Faron Pharmaceuticals. MH is currently employed by Faron Pharmaceuticals.

Patient consent for publication Not applicable.

Ethics approval The study was approved by the Ethics Committee of the Hospital District of Southwest Finland (ETMK 132/2016 and ETMK 34/1801/2021) and was conducted in accordance with the ethical principles of the Declaration of Helsinki. Written informed consent was obtained from each participant.

Provenance and peer review Not commissioned; externally peer reviewed.

Data availability statement Data are available in a public, open access repository. Data are available on reasonable request. The data sets generated during the current study are available in the Gene Expression Omnibus (GEO, https://www.ncbi.nlm.nih.gov/geo/). The RNA-seq and scRNA-seq data reported in this study have been deposited in GEO under accession numbers GSE292823 and GSE292824, respectively. Other types of data will be shared by MH (maijal@utu.fi) on reasonable request.

ORCID iDs
Jenna H Rannikko http://orcid.org/0000-0002-9506-9099
Maija Hollmén http://orcid.org/0000-0002-3250-7653

REFERENCES

1 Mantovani A, Allavena P, Marchesi F, *et al*. Macrophages as tools and targets in cancer therapy. *Nat Rev Drug Discov* 2022;21:799–820.
2 Goswami S, Anandhan S, Raychaudhuri D, *et al*. Myeloid cell-targeted therapies for solid tumours. *Nat Rev Immunol* 2023;23:106–20.
3 Rannikko JH, Hollmén M. Clinical landscape of macrophage-reprogramming cancer immunotherapies. *Br J Cancer* 2024;131:627–40.
4 Ma RY, Black A, Qian BZ. Macrophage diversity in cancer revisited in the era of single-cell omics. *Trends Immunol* 2022;43:546–63.
5 Mulder K, Patel AA, Kong WT, *et al*. Cross-tissue single-cell landscape of human monocytes and macrophages in health and disease. *Immunity* 2021;54:1883–900.
6 Laviron M, Petit M, Weber-Delacroix E, *et al*. Tumor-associated macrophage heterogeneity is driven by tissue territories in breast cancer. *Cell Rep* 2022;39:110865.
7 Matusiak M, Hickey JW, van IJzendoorn DGP, *et al*. Spatially Segregated Macrophage Populations Predict Distinct Outcomes in Colon Cancer. *Cancer Discov* 2024;14:1418–39.
8 Hollmén M, Figueiredo CR, Jalkanen S. New tools to prevent cancer growth and spread: a “Clever” approach. *Br J Cancer* 2020;123:501–9.
9 Rannikko JH, Verlingue L, de Miguel M, *et al*. Bexmarilimab-induced macrophage activation leads to treatment benefit in solid tumors: The phase I/II first-in-human MATINS trial. *Cell Rep Med* 2023;4:101307.
10 Kontro M, Stein AS, Pyörälä M, *et al*. Encouraging Efficacy of Bexmarilimab with Azacitidine in Relapsed or Refractory MDS in Bexmab Ph1/2 Study. *Blood* 2024;144:4265.
11 Hollmén M, Maksimow M, Rannikko JH, *et al*. Nonclinical Characterization of Bexmarilimab, a Clever-1-Targeting Antibody

for Supporting Immune Defense Against Cancers. *Mol Cancer Ther* 2022;21:1207–18.
12 Virtakoivu R, Rannikko JH, Viitala M, *et al*. Systemic Blockade of Clever-1 Elicits Lymphocyte Activation Alongside Checkpoint Molecule Downregulation in Patients with Solid Tumors: Results from a Phase I/II Clinical Trial. *Clin Cancer Res* 2021;27:4205–20.
13 Rannikko JH, Bono P, Hynninen J, *et al*. Bexmarilimab Activates Human Tumor-Associated Macrophages to Support Adaptive Immune Responses in Interferon-Poor Immune Microenvironments. *Cancer Immunol Res* 2024;12:48–59.
14 Thorsson V, Gibbs DL, Brown SD, *et al*. The Immune Landscape of Cancer. *Immunity* 2018;48:812–30.
15 Jenkins RW, Aref AR, Lizotte PH, *et al*. *Ex Vivo* Profiling of PD-1 Blockade Using Organotypic Tumor Spheroids. *Cancer Discov* 2018;8:196–215.
16 Voabil P, de Bruijn M, Roelofsen LM, *et al*. An ex vivo tumor fragment platform to dissect response to PD-1 blockade in cancer. *Nat Med* 2021;27:1250–61.
17 Turpin R, Peltonen K, Rannikko JH, *et al*. Patient-derived tumor explant models of tumor immune microenvironment reveal distinct and reproducible immunotherapy responses. *Oncoimmunology* 2025;14:2466305.
18 Viitala M, Virtakoivu R, Tadayon S, *et al*. Immunotherapeutic Blockade of Macrophage Clever-1 Reactivates the $CD8^+$ T-cell Response against Immunosuppressive Tumors. *Clin Cancer Res* 2019;25:3289–303.
19 Rusinova I, Forster S, Yu S, *et al*. Interferome v2.0: an updated database of annotated interferon-regulated genes. *Nucleic Acids Res* 2013;41:D1040–6.
20 Liberzon A, Birger C, Thorvaldsdóttir H, *et al*. The Molecular Signatures Database (MSigDB) hallmark gene set collection. *Cell Syst* 2015;1:417–25.
21 Shenoy AR, Wellington DA, Kumar P, *et al*. GBP5 promotes NLRP3 inflammasome assembly and immunity in mammals. *Science* 2012;336:481–5.
22 Guilliams M, Bruhns P, Saeys Y, *et al*. The function of Fcγ receptors in dendritic cells and macrophages. *Nat Rev Immunol* 2014;14:94–108.
23 Roumenina LT, Daugan MV, Petitprez F, *et al*. Context-dependent roles of complement in cancer. *Nat Rev Cancer* 2019;19:698–715.
24 Simmons DP, Nguyen HN, Gomez-Rivas E, *et al*. SLAMF7 engagement superactivates macrophages in acute and chronic inflammation. *Sci Immunol* 2022;7:eabf2846.
25 House IG, Savas P, Lai J, *et al*. Macrophage-Derived CXCL9 and CXCL10 Are Required for Antitumor Immune Responses Following Immune Checkpoint Blockade. *Clin Cancer Res* 2020;26:487–504.
26 Weng J, Wang Z, Hu Z, *et al*. Repolarization of Immunosuppressive Macrophages by Targeting SLAMF7-Regulated CCL2 Signaling Sensitizes Hepatocellular Carcinoma to Immunotherapy. *Cancer Res* 2024;84:1817–33.
27 Qu Y, Wen J, Thomas G, *et al*. Baseline Frequency of Inflammatory Cxcl9-Expressing Tumor-Associated Macrophages Predicts Response to Avelumab Treatment. *Cell Rep* 2020;32:107873.
28 Joo V, Petrovas C, de Leval L, *et al*. A CD64/FcγRI-mediated mechanism hijacks PD-1 from PD-L1/2 interaction and enhances anti-PD-1 functional recovery of exhausted T cells. *Front Immunol* 2023;14:1213375.
29 Rantakari P, Patten DA, Valtonen J, *et al*. Stabilin-1 expression defines a subset of macrophages that mediate tissue homeostasis and prevent fibrosis in chronic liver injury. *Proc Natl Acad Sci USA* 2016;113:9298–303.
30 Karikoski M, Marttila-Ichihara F, Elima K, *et al*. Clever-1/stabilin-1 controls cancer growth and metastasis. *Clin Cancer Res* 2014;20:6452–64.
31 Onkar S, Cui J, Zou J, *et al*. Immune landscape in invasive ductal and lobular breast cancer reveals a divergent macrophage-driven microenvironment. *Nat Cancer* 2023;4:516–34.
32 van Elsas MJ, Middelburg J, Labrie C, *et al*. Immunotherapy-activated T cells recruit and skew late-stage activated M1-like macrophages that are critical for therapeutic efficacy. *Cancer Cell* 2024;42:1032–50.
33 Sharma P, Siddiqui BA, Anandhan S, *et al*. The Next Decade of Immune Checkpoint Therapy. *Cancer Discov* 2021;11:838–57.
34 Reijers ILM, Rao D, Versluis JM, *et al*. IFN-γ signature enables selection of neoadjuvant treatment in patients with stage III melanoma. *J Exp Med* 2023;220:e20221952.
35 Ayers M, Lunceford J, Nebozhyn M, *et al*. IFN-γ-related mRNA profile predicts clinical response to PD-1 blockade. *J Clin Invest* 2017;127:2930–40.
36 Nalio Ramos R, Missolo-Koussou Y, Gerber-Ferder Y, *et al*. Tissue-resident $FOLR2^+$ macrophages associate with $CD8^+$ T cell infiltration in human breast cancer. *Cell* 2022;185:1189–207.
37 Stout RD, Jiang C, Matta B, *et al*. Macrophages sequentially change their functional phenotype in response to changes in microenvironmental influences. *J Immunol* 2005;175:342–9.
38 Guilliams M, Svedberg FR. Does tissue imprinting restrict macrophage plasticity? *Nat Immunol* 2021;22:118–27.
39 Subramanian S, Busch CJ-L, Molawi K, *et al*. Long-term culture-expanded alveolar macrophages restore their full epigenetic identity after transfer in vivo. *Nat Immunol* 2022;23:458–68.
40 Malani D, Kumar A, Brück O, *et al*. Implementing a Functional Precision Medicine Tumor Board for Acute Myeloid Leukemia. *Cancer Discov* 2022;12:388–401.
41 Kornauth C, Pemovska T, Vladimer GI, *et al*. Functional Precision Medicine Provides Clinical Benefit in Advanced Aggressive Hematologic Cancers and Identifies Exceptional Responders. *Cancer Discov* 2022;12:372–87.
42 Turpin R, Liu R, Munne PM, *et al*. Respiratory complex I regulates dendritic cell maturation in explant model of human tumor immune microenvironment. *J Immunother Cancer* 2024;12:e008053.
43 Han Y, Guo Z, Jiang L, *et al*. CXCL10 and CCL5 as feasible biomarkers for immunotherapy of homologous recombination deficient ovarian cancer. *Am J Cancer Res* 2023;13:1904–22.
44 Kang K, Bachu M, Park SH, *et al*. IFN-γ selectively suppresses a subset of TLR4-activated genes and enhancers to potentiate macrophage activation. *Nat Commun* 2019;10:3320–.
45 Benci JL, Xu B, Qiu Y, *et al*. Tumor Interferon Signaling Regulates a Multigenic Resistance Program to Immune Checkpoint Blockade. *Cell* 2016;167:1540–54.
46 Gocher AM, Workman CJ, Vignali DAA. Interferon-γ: teammate or opponent in the tumour microenvironment? *Nat Rev Immunol* 2022;22:158–72.
47 Yi M, Li T, Niu M, *et al*. Targeting cytokine and chemokine signaling pathways for cancer therapy. *Signal Transduct Target Ther* 2024;9:176.
48 Das S, Johnson DB. Immune-related adverse events and anti-tumor efficacy of immune checkpoint inhibitors. *J Immunother Cancer* 2019;7:306.
49 Young A, Quandt Z, Bluestone JA. The Balancing Act between Cancer Immunity and Autoimmunity in Response to Immunotherapy. *Cancer Immunol Res* 2018;6:1445–52.
50 Dunkel J, Viitala M, Karikoski M, *et al*. Enhanced Antibody Production in Clever-1/Stabilin-1-Deficient Mice. *Front Immunol* 2018;9:2257.